Title

Rhein targets macrophage SIRT2 to promote adipose tissue thermogenesis in obesity in mice.

Journal

Communications Biology, 7(1)

Authors

Zhou, Ruo-Nan
Zhu, Zi-Wei
Xu, Ping-Yuan
et al.

Publication Date

2024-08-16

DOI

10.1038/s42003-024-06693-6

Peer reviewed

communications biology

Article

https://doi.org/10.1038/s42003-024-06693-6

Rhein targets macrophage SIRT2 to promote adipose tissue thermogenesis in obesity in mice

Ruo-Nan Zhou[1,2], Zi-Wei Zhu[1,2], Ping-Yuan Xu[1,2], Li-Xuan Shen[1,2], Ziwei Wang[1,2], Ying-Ying Xue[1,2], Ying-Ying Xiang[1,2], Yue Cao[1,2], Xi-Zhong Yu[2], Juan Zhao[2], Yu Jin[2], Jing Yan[2], Qin Yang[3], Peng-Hua Fang[2] ✉ & Wen-Bin Shang[1,2] ✉

Rhein, a component derived from rhubarb, has been proven to possess anti-inflammatory properties. Here, we show that rhein mitigates obesity by promoting adipose tissue thermogenesis in diet-induced obese mice. We construct a macrophage-adipocyte co-culture system and demonstrate that rhein promotes adipocyte thermogenesis through inhibiting NLRP3 inflammasome activation in macrophages. Moreover, clues from acetylome analysis identify SIRT2 as a potential drug target of rhein. We further verify that rhein directly interacts with SIRT2 and inhibits NLRP3 inflammasome activation in a SIRT2-dependent way. Myeloid knockdown of SIRT2 abrogates adipose tissue thermogenesis and metabolic benefits in obese mice induced by rhein. Together, our findings elucidate that rhein inhibits NLRP3 inflammasome activation in macrophages by regulating SIRT2, and thus promotes white adipose tissue thermogenesis during obesity. These findings uncover the molecular mechanism underlying the anti-inflammatory and anti-obesity effects of rhein, and suggest that rhein may become a potential drug for treating obesity.

Metabolic inflammation is implicated in the pathogenesis of various metabolic diseases, especially obesity[1,2]. Increasing attempts have been made to explore the approaches to modulate inflammation in the context of obesity in order to develop effective therapeutic strategies for both obesity and its complications[3]. *Rheum* L. (rhubarb) is consumed as an ingredient in cuisines or herbal remedies in many regions and has been proven to be beneficial for a wide range of inflammatory diseases, such as chronic kidney disease, sepsis and cancer[4]. Rhein is one of the major active components of rhubarb, which is also the active metabolite of diacerein, an FDA-approved anti-inflammatory drug for treating osteoarthritis (oral diacerein undergoes complete deacetylation to rhein in animals and humans)[5]. Recently, there have been several studies reporting that rhein reduces body weight in rodents with diet-induced obesity (DIO)[6–8]. However, the exact mechanism underlying the anti-inflammation and anti-obesity effects of rhein remains unclear.

It has been widely accepted that decreasing the production of interleukin-1β (IL-1β) is the most prominent characteristic of the anti-inflammatory activity of rhein and diacerein[5,9], and the NOD-, LRR-, and pyrin domain-containing 3 (NLRP3) inflammasome is now considered to be a main source of mature IL-1β[10]. The opinion from previous studies is that rhein blunts NLRP3 activation mainly through inhibiting nuclear factor-κB (NF-κB) activation in the priming step[11–13]. However, the results from both our research and that of others suggest that short-term treatment with rhein on macrophages reduces the NLRP3 inflammasome activation without changing the expression of NLRP3 or pro-IL-1β in cell lysates, suggesting the existence of a potential mechanism by which rhein directly inhibits the assembly of NLRP3 inflammasome without affecting the priming stage in macrophages[14]. Meanwhile, macrophages are the most plentiful immune cells in the adipose tissue and are crucial mediators of adipose tissue inflammation during obesity[15]. It was reported that, in obesity, multiple components of metabolism-associated molecular patterns (MAMPs) activate the NLRP3 inflammasome in adipose tissue macrophages (ATMs), inducing the expression of monoamine oxidase A (MAOA) which is responsible for norepinephrine (NE) degradation[16,17]. Elevated MAOA expression in ATMs reduces the local NE level to impair adipose tissue thermogenesis. Taken together, we hypothesize that promoting adipose tissue thermogenesis by inhibiting the assembly of NLRP3 inflammasome in ATMs may underlie the anti-obesity property of rhein.

In this study, we show that rhein promotes white adipose tissue thermogenesis by inhibiting NLRP3 inflammasome activation in macrophages.

[1]Department of Endocrinology, Jiangsu Province Hospital of Chinese Medicine, the Affiliated Hospital of Nanjing University of Chinese Medicine, Nanjing, 210029, China. [2]Key Laboratory for Metabolic Diseases in Chinese Medicine, Nanjing University of Chinese Medicine, Nanjing, 210023, China. [3]Department of Medicine, Physiology and Biophysics, University of California, Irvine, CA, 92697, USA. ✉e-mail: fphlcollegesci@njucm.edu.cn; wbshang@njucm.edu.cn

With acetylome analysis, we further identify SIRT2 as a drug target of rhein, as rhein directly binds to SIRT2 and inhibits the activation of NLRP3 inflammasome as well as the subsequent metabolic disorders in an SIRT2-dependent manner. Our findings reveal the molecular mechanism underlying the anti-inflammation as well as the anti-obesity properties of rhein.

Results

Rhein reduces obesity and improves insulin sensitivity

The existing studies on rhein in treating animal models of obesity adopted doses much higher than the clinically recommended dosage of diacerein[5,6,8,18–20]. Excessive intake of rhein may lead to adverse reactions, especially diarrhea, which interferes with the observation of metabolism status[21]. So, we gavaged rhein at 10 mg/kg per day to DIO mice for 4 weeks. The dosage of rhein is converted from the clinically advised dosage of diacerein. The mice showed significantly less weight gain after 4 weeks of rhein treatment (Fig. 1a, b; Fig. S1c), with obviously reduced white adipose tissue volume as well as redder interscapular brown adipose tissue (iBAT) (Fig. 1d, e; Fig. S1a). Hematoxylin-eosin (HE) staining also confirmed that the adipocyte diameters of both inguinal white adipose tissue (iWAT) and epididymis white adipose tissue (eWAT) were significantly smaller in the HFD + Rhe group than the HFD group (Fig. 1f; Fig. 1i). Compared with the HFD group, a decrease in the weight of iWAT, eWAT, iBAT and liver was observed in the mice from the HFD+Rhein group, though the difference is not statistically significant (Fig. S1b).

Insulin resistance, along with disruption of glucose and lipid homeostasis, are the prominent detrimental actions of obesity, so we investigated whether rhein could normalize these parameters[22]. As shown in Fig. 1, compared with the HFD group, the mice treated with rhein showed an obviously lower fasting blood glucose level (Fig. 1c) as well as a better tolerance to glucose load (Fig. 1g; Fig. 1j), and were more sensitive to insulin injection (Fig. 1h; Fig. 1k). Non-esterified fatty acid (NEFA) is the necessary substrate for triglyceride synthesis as well as an intermediate product of

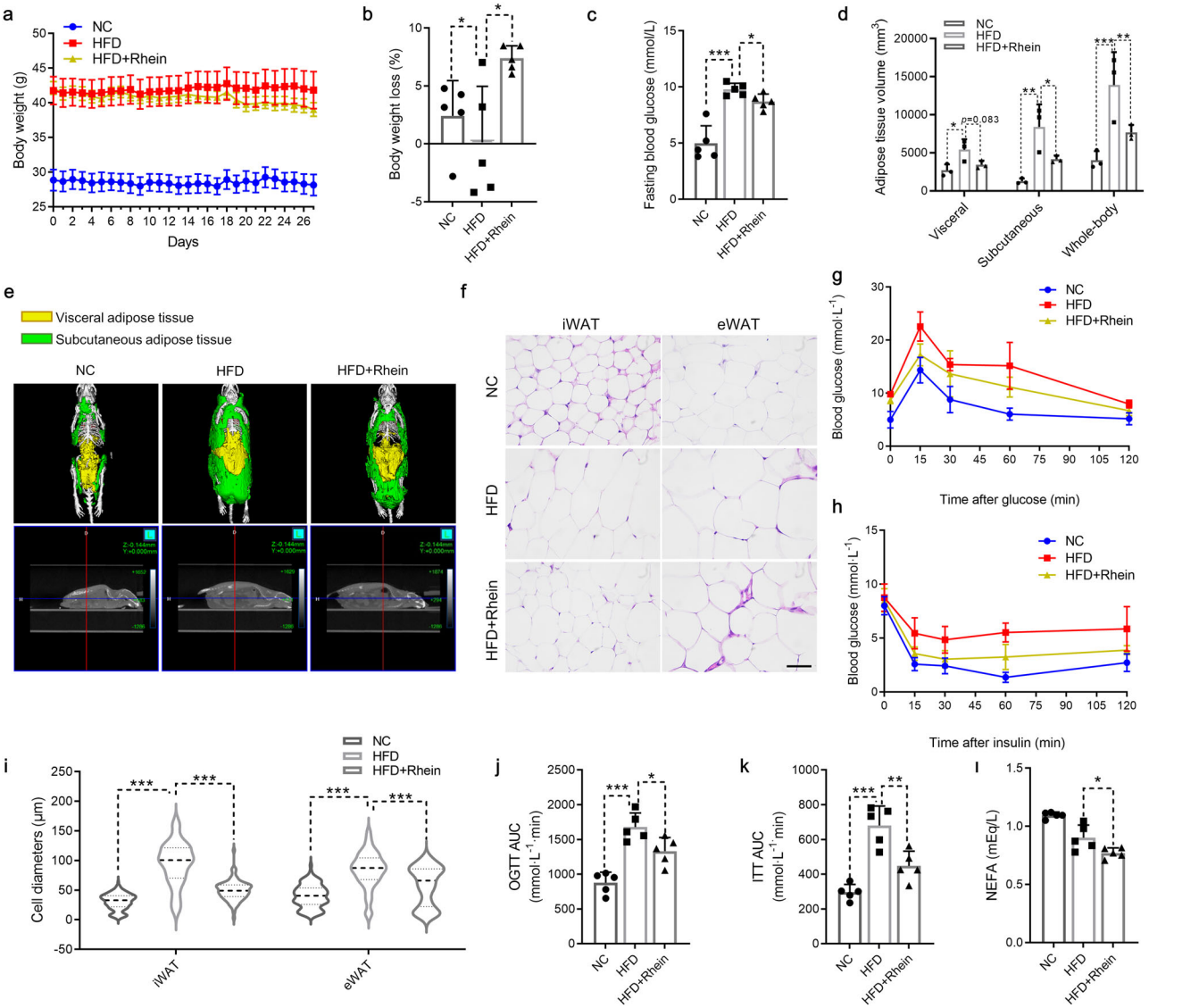

Fig. 1 | Rhein decreases weight gain and enhances insulin sensitivity in DIO mice. **a** Daily body weight of DIO mice during rhein treatment ($n = 5$). **b** Percentage of body weight loss after 28-day rhein treatment of DIO mice ($n = 5$). **c** Fasting blood glucose levels after 28-day rhein treatment of DIO mice ($n = 5$). **d**, **e** Representative micro-CT scan of DIO mice (**e**) and adipose tissue volume of DIO mice measured by micro-CT (**d**) ($n = 3$). **f**, **i** Representative H&E staining of dissected tissues (**f**) (scale bar, 50 μm) and quantification of adipocyte diameter of iWAT and eWAT (**i**) ($n = 3$). **g**, **j** Oral glucose tolerance test on DIO mice after a 12-h fast (**g**) and bar graph represents the average area under the curve (**j**) ($n = 5$). **h**, **k** i.p. insulin tolerance on DIO mice after 6-hour fast (**h**) and bar graph represents the average area under the curve (**k**) ($n = 5$). **l** Serum non-esterified fatty acid (NEFA) level of DIO mice after a 12-h fast ($n = 5$). Data are presented as the mean ± standard error (SD). Significance is indicated by $^{*}p < 0.05$, $^{**}p < 0.01$. and $^{***}p < 0.001$ compared to the corresponding group.

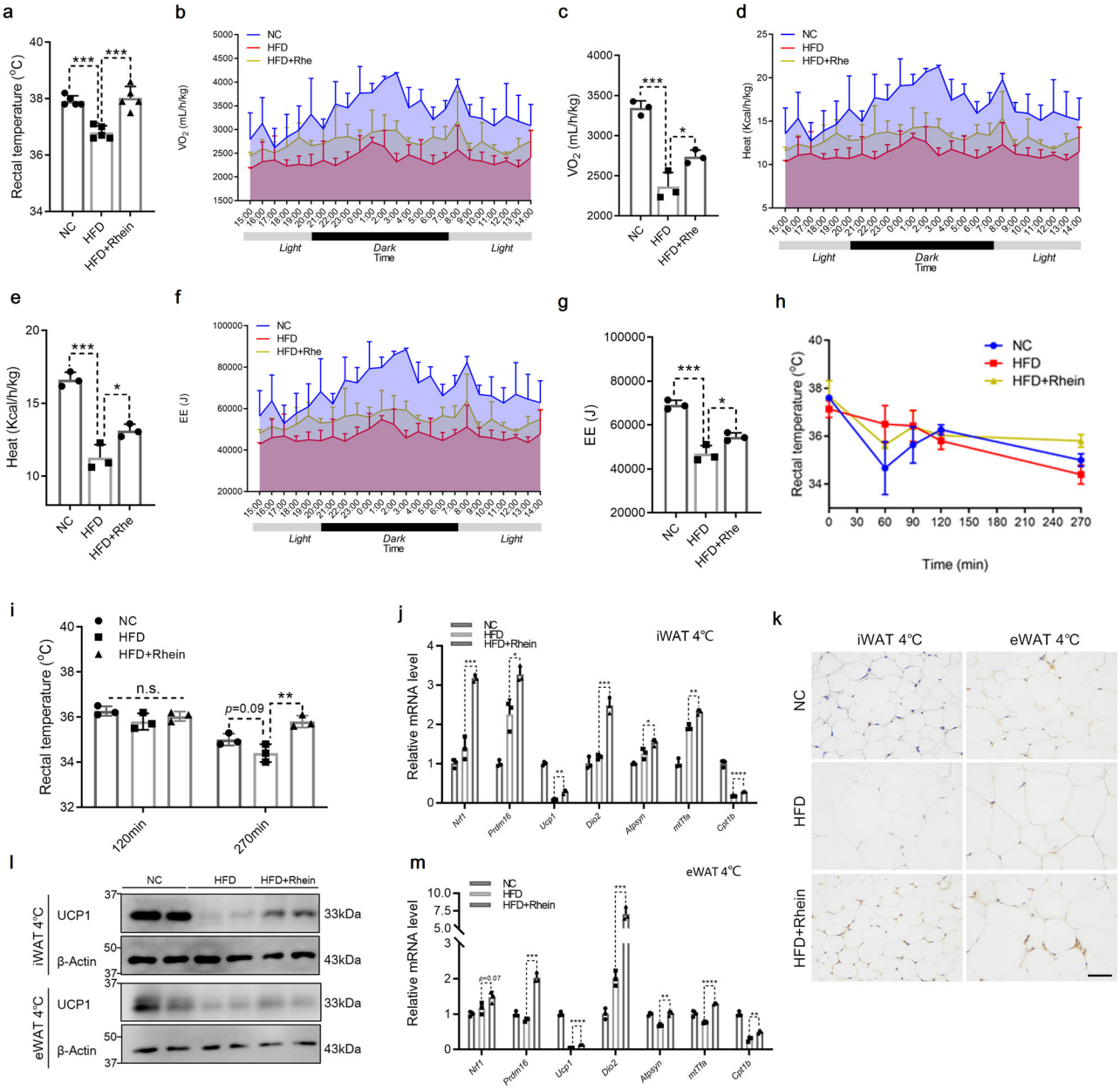

Fig. 2 | Rhein promotes white adipose tissue thermogenesis as well as whole-body energy expenditure in DIO mice. a Rectal temperature of DIO mice measured under room temperature after a 12-h fast ($n = 5$). **b**–**g** Energy expenditure measured by 24-h animal monitoring system. **b** oxygen consumption (VO2) and **d** heat production of DIO mice were normalized by body weight. **f** The energy expenditure (EE) was calculated following the Weir equation. The bar graphs represent the average of each group (**c** for **b**, **e** for **d** and **g** for **f**) ($n = 3$). **h**, **i** Rectal temperature variation during 270-min cold exposure. **h** Rectal temperature recorded during cold exposure. **i** The average rectal temperature of each group at the time point of 120 min and 270 min ($n = 3$). **j**, **m** Gene expression profiles in iWAT (**j**) and eWAT (**m**) after 270 min of cold exposure ($n = 3$). **k** Representative UCP1 immunohistochemical staining in iWAT and eWAT of DIO mice. Scale bar, 50 μm. **l** Immunoblots of UCP1 in iWAT and eWAT after 270 min of cold exposure. Data are presented as the mean ± SD. Significance is indicated by $^{*}p < 0.05$, $^{**}p < 0.01$ and $^{***}p < 0.001$ compared to the corresponding group. n.s. indicates no significance.

lipolysis[23]. We also investigated the NEFA level in the serum of all groups and observed a significant decline in NEFA after rhein treatment (Fig. 1l).

During the 4 weeks of rhein treatment, no obvious difference was observed in the fecal shape between the HFD group and the HFD+Rhe group, nor in 24 h food/water intake or physical activity (Fig. S1d, f, n), indicating that rhein was well-tolerated and the weight-reducing efficacy was not due to the gastrointestinal reactions caused by the anthraquinone scaffold of rhein (Fig. S1j)[5,24]. Moreover, we also observed an elevated fasting rectal temperature in rhein-treated mice (Fig. 2a). All the evidence above suggests that the beneficial effects of rhein on combating obesity might be relevant to an increase in energy expenditure.

Rhein increases the thermogenic capability of white adipose tissue in DIO mice

To further observe the influence of rhein on energy expenditure, we housed mice from all groups into metabolic cages for a 24-h analysis. After normalizing to body weight, the rhein-treated mice exhibited a remarkably higher oxygen consumption (Fig. 2b, c) and carbon dioxide production rate (Fig. S1g, h) than the mice from the HFD group. Consistent with the above, the mice receiving rhein treatment showed a noticeable increase in whole-body energy expenditure (Fig. 2d–g).

Seeing that rhein influenced neither calorie intake nor physical activity but elevated the rectal temperature, we hypothesized that the adipose tissue

thermogenesis might be responsible for the elevated energy expenditure. To gauge adipose tissue thermogenesis, we employed a 270-minute cold tolerance test. At 270 min, the mice receiving rhein treatment acquired a significantly higher core body temperature than the mice from the HFD group (Fig. 2h, i). Uncoupling protein-1 (UCP1) is widely recognized as the main thermogenic effector. Adipose tissue thermogenesis chiefly relies on the uncoupling of mitochondrial oxidative phosphorylation induced by a UCP1-dependent proton leak[25]. We further checked the gene and protein expression of UCP1 in different types of adipose tissues. The results showed that HFD impaired while rhein treatment rescued the UCP1 expression in both iWAT and eWAT (Fig. 2k, l; Fig. S1l, m), meanwhile, we also observed that rhein treatment strongly activated genes related to adipose tissue thermogenesis (*Nrf1, Prdm16, Dio2, mtTfa, Atpsyn and Cpt1b*) in both iWAT and eWAT (Fig. 2j, m).

However, although we noticed that HFD gave rise to the whitening of brown adipose tissue while rhein treatment impeded this process (Fig. S1i), rhein did not change the expression of UCP1 compared to the HFD group (Fig. S1k). Evidence from earlier studies[26] and our results both suggest that though HFD is an inducing factor of brown adipose tissue whitening, it increases the expression of UCP1 in brown adipose tissue (Fig. S1k). The specific mechanism underlying the phenomenon is still undetermined. Combining the fact that rhein did not alter the expression of UCP1 in brown adipose tissue, we took only white adipose tissue as the target organ of rhein for further exploration in this study.

Rhein-suppressed NLRP3-induced MAOA expression in macrophages

Considering that the activation of NLRP3 inflammasome in ATMs plays a fundamental role in adipose tissue thermogenesis, and rhein is a representative anti-inflammatory drug, we identified the activation of NLRP3 in iWAT and eWAT. As shown in the results, compared with the HFD group, the markers of NLRP3 activation, Caspase1 p20 and IL-1β p17, were profoundly decreased in the HFD+Rhe group (Fig. 3a), which indicates that rhein treatment inhibits NLRP3 inflammasome activation in the white adipose tissue of DIO mice.

To elucidate whether rhein rescues adipose tissue thermogenesis in a NLRP3-MAOA dependent manner, we detected MAOA expression in adipose tissues and found that rhein treatment significantly downregulated the expression of MAOA in both iWAT and eWAT (Fig. 3a).

We further used lipopolysaccharide (LPS) combined with adenosine triphosphate (ATP) to induce the activation of NLRP3 inflammasome in bone marrow-derived macrophages (BMDMs) and treated the cells with rhein. The results showed that rhein inhibited the IL-1β secretion (Fig. 3b; Fig. S2a), along with the formation of ASC specks (Fig. 3d, g) and the cell pyroptosis (Fig. 3e, f) induced by LPS + ATP, which suggests that rhein inhibits the activation of NLRP3 inflammasome in BMDMs. Most importantly, we observed that rhein reduced the high expression of MAOA induced by the activation of NLRP3 inflammasome in BMDMs (Fig. 3c). Similarly, in the J774A.1 macrophage cell line, rhein inhibited the activation of NLRP3 inflammasome and reduced the MAOA expression (Fig. 3h–j; Fig. S2b). However, in J774A.1 cell with *Nlrp3* knocked down using interfering RNA (si-RNA), rhein failed to repress *Maoa* expression on neither the mRNA nor protein level (Fig. 3I, j; Fig. S2c). These results suggest that rhein reduces the expression of MAOA in an NLRP3-dependent way.

Additionally, we also observed that rhein blunted the NLRP3 activation triggered by nigericin and monosodium urate crystals (MSU) in BMDMs, which indicates that the inhibition of NLRP3 inflammasome by rhein is irrelevant to the type of stimuli (Fig. S2d, e).

Rhein regulates adipose tissue thermogenesis in a macrophage NLRP3-dependent manner

To further clarify the relationship between the effects of rhein on adipose tissue thermogenesis and NLRP3 inflammasome activation in macrophages, we constructed an adipocyte-macrophage co-culture system (Fig. 4a). Briefly, BMDMs were seeded in the culture inserts and stimulated by LPS + ATP with or without rhein treatment before co-culture. The corresponding amount of NE was added to the mature white adipocytes induced from the stromal-vascular fraction (SVF) of mouse inguinal adipose tissue or the 3T3-L1 cell line right before co-culture. Then co-culture the BMDMs and the adipocytes for 1 h.

Due to the difference in NE sensitivity between primary white adipocytes (primary WAC) and 3T3-L1 derived adipocytes (3T3-L1), We first employed a NE gradient to treat the adipocytes and obtained the response curve of *Ucp1* mRNA to NE (Fig. 4b, c). Based on the results obtained, we chose 0.5 μM NE to treat primary WAC and 10 μM NE to treat 3T3-L1, respectively.

Mitochondrial membrane potential is the main driver of ATP synthesis or UCP1-mediated proton leak[27]. We thereby used tetramethylrhodamine ethyl ester perchlorate (TMRE) dye to estimate the mitochondrial membrane potentials in adipocytes after co-culture. The results showed that in both primary WAC and 3T3-L1, treatment of rhein on BMDMs apparently increased the fluorescence intensity of TMRE in adipocytes (Fig. 4d, e; Fig. S3a, b). We also detected the expression of thermogenesis-related genes in primary WAC and 3T3-L1. As expected, the treatment of rhein on BMDMs increased the expression of *Ucp1* and *mtTfa* in primary WAC while elevating the expression of *Ucp1*, *Dio2*, *mtTfa*, *Atpsyn*, *Mcad* and *Cpt1b* in 3T3-L1 (Fig. 4h, i). These results indicate that the rhein treatment on NLRP3-activated macrophages boosts the thermogenesis in adipocytes co-cultured with these macrophages.

We also used NLRP3-unactivated BMDMs to co-culture with adipocytes (Fig. 4f, g, lane 1 and lane 2; Fig. S3c, d). The results showed that rhein treatment on BMDMs changed neither the expression of UCP1 nor phospho-PKA (p-PKA) substrates in adipocytes under the condition that NLRP3 was not activated in BMDMs. These results indicate that the activation of NLRP3 inflammasome in macrophages is necessary for rhein-induced adipocyte thermogenesis.

Considering that MAOA inhibitors have a direct impact on adipocyte lipid metabolism, we next administered the co-culture using adipocytes untreated with NE. As shown in the results (Fig. 4f, g, lane 5 and lane 6; Fig. S3c, d), the expression of UCP1 or p-PKA substrates in adipocytes was not changed. This result illustrates that the presence of NE is required for rhein to promote adipocyte thermogenesis and implies the participation of macrophage MAOA in rhein-induced adipocyte thermogenesis. Taken together, our results indicate that rhein regulates adipose tissue thermogenesis by inhibiting the activation of NLRP3 inflammasome in ATMs.

Rhein inhibits NLRP3 inflammasome activation by influencing SIRT2-induced acetylation

It is widely believed that two steps are required for NLRP3 inflammasome activation. During the priming stage, the activation of NF-κB induces gene transcription of NLRP3 and pro-IL-1β. In the assembly stage, ASC is recruited to NLRP3 for the cleavage of pro-caspase-1. Activated caspase-1 further cleaves pro-IL-1β and pro-interleukin-18 (pro-IL-18) into mature IL-1β and IL-18 for release[28]. Earlier studies are of the opinion that rhein blunts NLRP3 activation mainly by inhibiting NF-κB activation in the priming step[11–13]. However, as shown in Fig. 3c and Fig. 3j, 30 min of rhein treatment frustrated the activation of NLRP3 inflammasome while having no significant influence on the expression of NLRP3 and pro-IL-1β in both BMDMs and J774A.1 macrophages. So, we further checked the TNF-α secretion, another iconic inflammatory factor downstream of NF-κB in both BMDMs and J774A.1 cells. Consistent with the results of NLRP3 and pro-IL-1β, 30-min treatment of rhein has no effect on TNF-α secretion in BMDMs and J774A.1 cells (Fig. 5a, b). Moreover, the immunofluorescent staining of the NF-κB p65 subunit also showed that 30 min of rhein treatment did not reduce the translocation of p65 from cytoplasmic to nuclear induced by LPS combined with ATP (Fig. S5i). All these evidences demonstrate that short-time treatment of rhein directly inhibits the activation of NLRP3 inflammasome without affecting the NF-κB pathway.

So, how does rhein inhibit the activation of NLRP3 inflammasome exactly? Given that the duration of rhein treatment was only 30 min, we

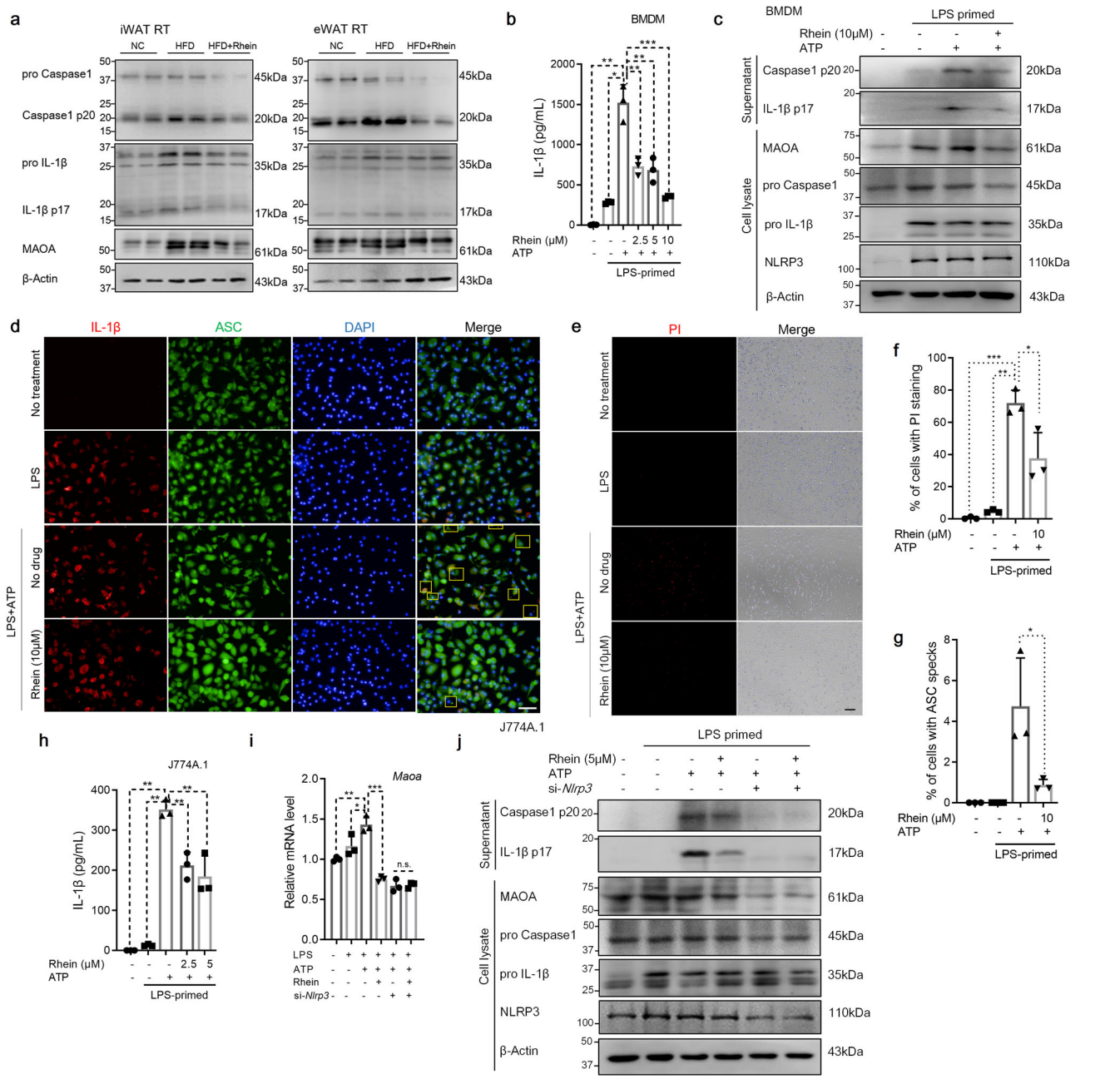

Fig. 3 | Rhein decreases NLRP3-dependent MAOA expression in macrophages. **a** Immunoblots of Caspase1, IL-1β, MAOA in the iWAT and eWAT of DIO mice under room temperature. **b**–**g** BMDMs were primed with LPS and then treated with rhein or DMSO for 0.5 h and finally stimulated with ATP. **b** IL-1β levels detected by ELISA in the supernatant of BMDMs. **c** Immunoblots of IL-1β p17, Caspase1 p20 in culture supernatant and pro IL-1β, pro Caspase1, NLRP3, MAOA in the cell lysate of BMDMs. **d** IL-1β and ASC immunofluorescent staining of BMDMs. Scale bar, 50 μm. **e** PI staining of BMDMs. Scale bar, 200 μm. **f** Percentage of PI-positive cells of each field. **g** Percentage of ASC specks of each field. **h** J774A.1 macrophages were primed with LPS and then treated with rhein or DMSO for 0.5 h and finally stimulated with ATP. IL-1β levels in the culture supernatant were detected by ELISA. **i**, **j** J774A.1 macrophages transfected with si-*Nlrp3* or si-*Scramble* were treated as (**h**). **i** *Maoa* expression measured by qRT-PCR. **j** Immunoblots of IL-1β p17, Caspase1 p20 in culture supernatant and pro IL-1β, pro Caspase1, NLRP3, MAOA in the cell lysate of J774A.1 macrophage. Data are presented as the mean ± SD. Significance is indicated by $^{*}p < 0.05$, $^{**}p < 0.01$, and $^{***}p < 0.001$ compared to the corresponding group. n.s. indicates no significance.

focused on the rapid biological processes that may affect NLRP3 activation, especially post-translational modifications (PTMs) of proteins. Post-translational modification refers to covalently binding functional groups on the amino acid residues of specific proteins, thereby adjusting the stability, activity, localization, and intermolecular interaction of these proteins. So far, the PTMs reported to influence NLRP3 inflammasome activation include phosphorylation, acetylation, ubiquitylation, and sumoylation[29]. We thus detected the levels of PTMs mentioned above in the whole-cell lysates of BMDMs and J774a.1 macrophages. As shown in Fig. 5c, rhein only decreased the acetylation level of NLRP3-activated macrophages. No significant difference was observed in phosphorylation, ubiquitylation, and sumoylation levels between rhein-treated and DMSO-treated macrophages, which infers that rhein may influence the activation of NLRP3 inflammasome by altering the state of acetylation in macrophages.

Enzymes are the main regulators of post-translational modifications. Acetylation of proteins is mainly catalyzed by lysine deacetylases (KDACs) and lysine acetyltransferases (KATs)[30]. Rhein may probably adjust the acetylation level of macrophages through these enzymes. In order to identify

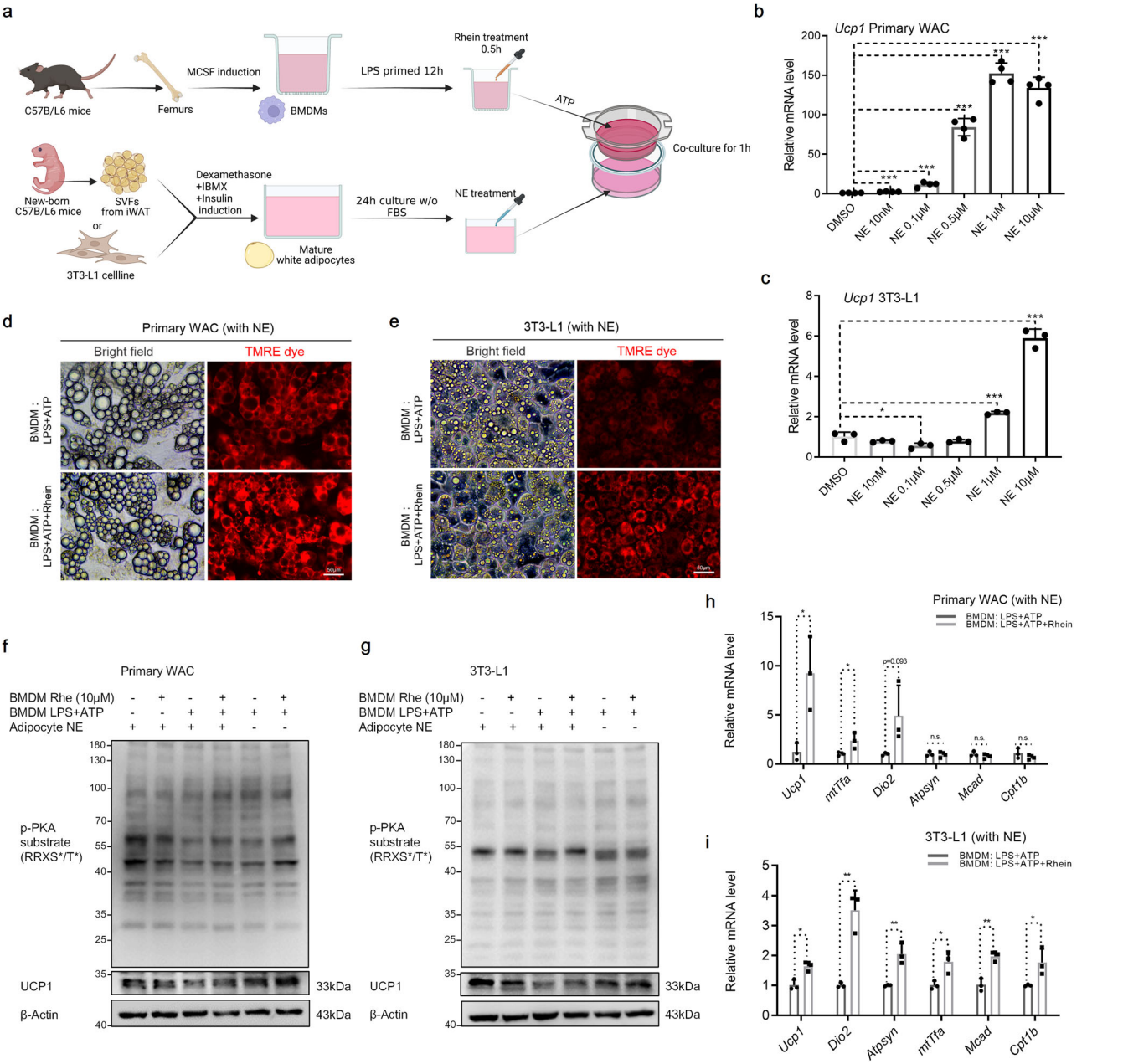

Fig. 4 | Rhein-mediated adipocyte thermogenesis is dependent upon the inhibition of NLRP3 inflammasome in macrophages. a The workflow of macrophage-adipocyte co-culture system. **b**, **c** *Ucp1* fold change measured by qRT-PCR in **b** primary white adipocytes and **c** 3T3-L1 derived adipocytes induced by NE gradient. **d**, **e** TMRE staining of NE stimulated **d** primary white adipocytes and **e** 3T3-L1 derived adipocytes co-cultured with NLRP3 activated BMDMs with or without rhein treatment, Scale bar, 50 μm. **f**, **g** Immunoblots of p-PKA substrate and UCP1 in **f** primary white adipocytes and **g** 3T3-L1 derived adipocytes co-cultured with BMDMs. **h**, **i** Gene expression profiles in NE stimulated **h** primary white adipocytes and **i** 3T3-L1 derived adipocytes co-cultured with NLRP3 activated BMDMs with or without rhein treatment. Data are presented as the mean ± SD. Significance is indicated by $^{*}p < 0.05$, $^{**}p < 0.01$, and $^{***}p < 0.001$ compared to the corresponding group. n.s. indicates no significance.

the specific enzyme responsible for the acetylation-adjusting as well as NLRP3-inhibiting effects of rhein, we employed an acetylome to analyze the total cell extracts from NLRP3-activated J774A.1 macrophages with or without rhein treatment (Fig. 5d). We totally identified 4581 acetylated sites from 1927 proteins in the proteome, wherein 158 acetylated sites of 152 proteins met the rule of significant difference ($p < 0.05$ with fold change > 1.5 or <0.67). In view of the fact that NLRP3 inflammasome activation happens mainly in the cytoplasm, we further gated 83 acetylated sites of 81 proteins residing in the cytoplasm and put these proteins into the STRING database with NLRP3 inflammasome components. Finally, we screened out 25 acetylated sites of 25 proteins altered significantly by rhein, residing in the cytoplasm and related to NLRP3 inflammasome components (Fig. 5e, f). We next put the cytoplasmic KDACs and KATs reported to have an influence on NLRP3 activation into the STRING database together with the 25 proteins and counted the number of proteins connected with each enzyme (Fig. S4e). As shown in Fig. 5g, sirtuin 2 (SIRT2) and histone deacetylase 6 (HDAC6), both obtained 9 connections, tied for the first place of the most connected enzymes. Intriguingly, it is reported that both SIRT2 and HDAC6 are capable of deacetylating α-tubulin, and the acetylation of α-tubulin directly mediates NLRP3 activation[31,32]. We accordingly gauged the acetylation of α-tubulin in BMDMs and found that LPS + ATP profoundly increased the acetylation of α-tubulin while rhein treatment dramatically

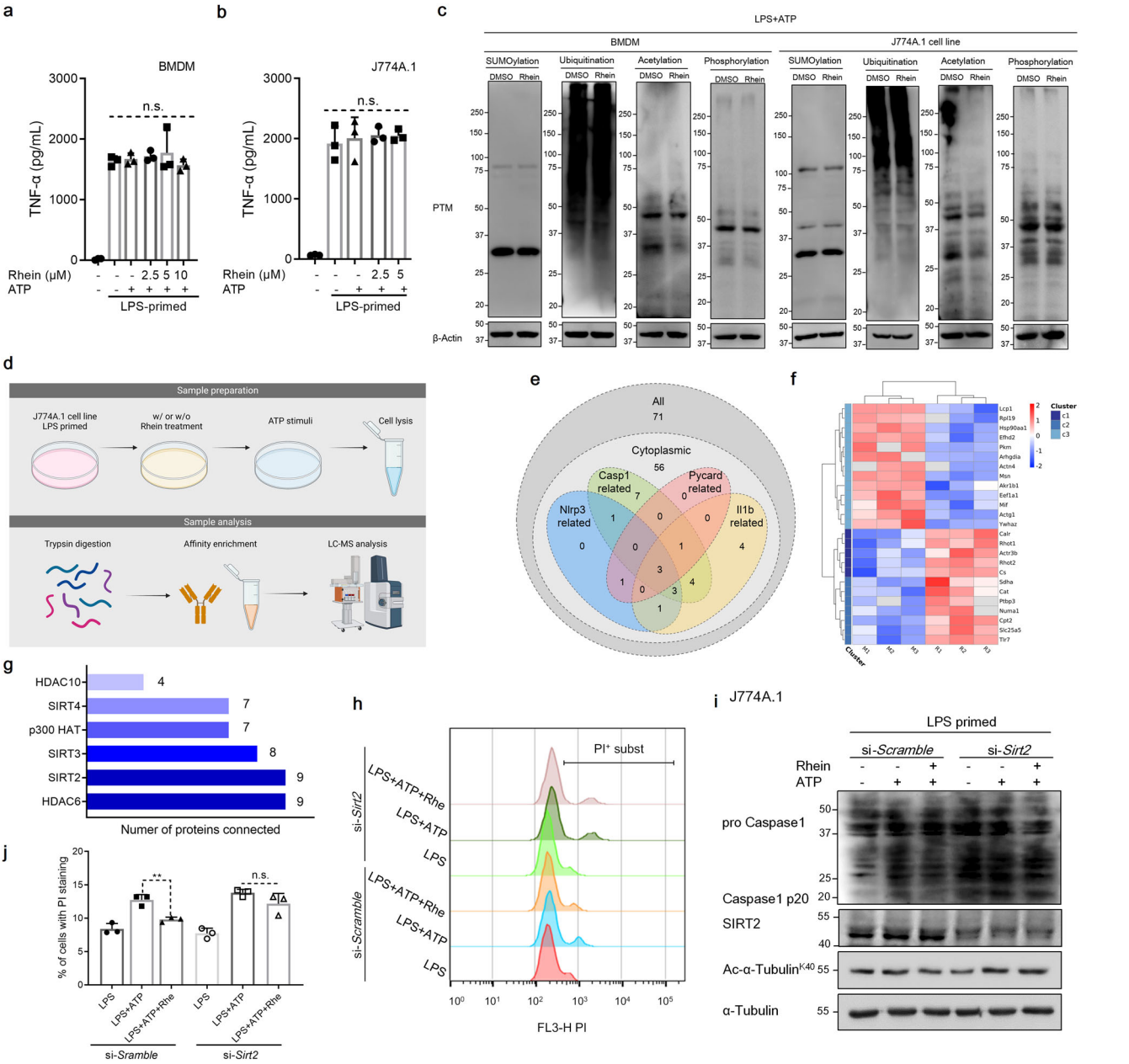

Fig. 5 | Rhein inhibits NLRP3 inflammasome activation in a SIRT2-dependent way. a, **b** TNF-α levels of (a) BMDMs and (b) J774A.1 macrophages primed with LPS and then treated with rhein or DMSO for 0.5 h and finally stimulated with ATP. **c** Immunoblots of phosphorylation, ubiquitylation, acetylation, and sumoylation levels in the cell lysate of BMDMs and J774A.1 macrophages treated as (**a**, **b**). **d** The workflow of acetylome analysis. **e** The Venn diagram of 152 proteins with a significant change of acetylation after rhein treatment. **f** Heat map of 25 NLRP3 inflammasome-related proteins among 152 proteins in (**e**). **g** Counts on connections of 25 proteins in **f** to NLRP3-related cytoplasmic acetylation modifying enzymes. **h–j** J774A.1 macrophages transfected with si-*Sirt2* or si-*Scramble* were primed with LPS and then treated with rhein or DMSO for 0.5 h and finally stimulated with ATP. **h** PI-positive cells were detected by flowcytometry. **i** Immunoblots of Caspase1, SIRT2 and acetylated α-Tubulin in cell lysate. **j** Percentage of PI-positive cells in (**h**). Data are presented as the mean ± SD. Significance is indicated by $^{**}p < 0.01$ compared to the corresponding group. n.s. indicates no significance.

reduced the acetylation of tubulin (Fig. S5a). Considering that SIRT2 inhibits while HDAC6 promotes the activation of NLRP3 inflammasome, we made the deduction that SIRT2 is more likely to be a pharmacological target of rhein.

To confirm our hypothesis, we knocked down *Sirt2* by si-*Sirt2* in J774A.1 macrophages and activated the NLRP3 inflammasome by LPS + ATP with or without rhein treatment in these cells. The results showed that the inhibitory capabilities of rhein on the activation of NLRP3 inflammasome (Fig. 5h–j; Fig. S5e) were impeded in *Sirt2* knocked-down J774A.1 macrophages. In addition, the knockdown of *Sirt2* also blunted the deacetylation of α-tubulin induced by rhein (Fig. 5i; Fig. S5c), which indicates that rhein inhibits NLRP3 inflammasome activation by SIRT2, and SIRT2-mediated α-tubulin acetylation is likely responsible for the inhibitory effect of rhein on NLRP3 inflammasome activation.

SIRT2 is a bona fide target of rhein

Although we have proved that rhein inhibits the activation of NLRP3 inflammasome in a SIRT2-dependent way, rhein did not alter the expression of SIRT2 in NLRP3-activated macrophages (Fig. 5i; Fig. S5d). Therefore, we used AGK2 (a SIRT2 inhibitor)-pre-treated BMDMs to examine the influence of SIRT2 activity on the inflammasome-inhibitory effect of rhein. As shown in Fig. 6a, b, pre-treatment of AGK2 impaired the

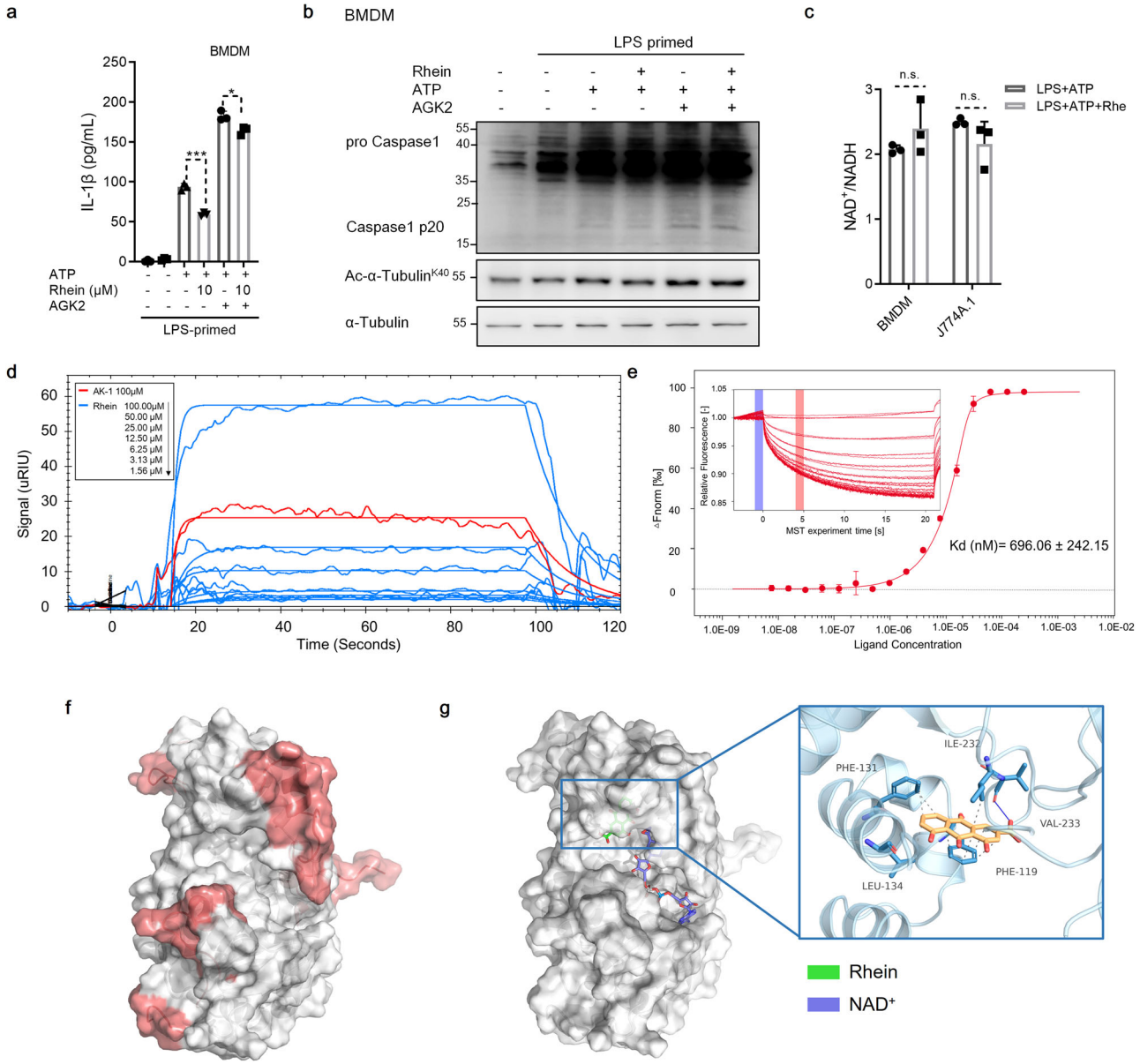

Fig. 6 | SIRT2 is a bona fide target of rhein. a, **b** BMDMs were primed with LPS and pretreated with SIRT2 inhibitor AGK2 for 2 h, and then treated with rhein or DMSO for 0.5 h and finally stimulated with ATP. **a** IL-1β levels detected by ELISA in the supernatant of BMDMs. **b** Immunoblots of Caspase1 and acetylated α-Tubulin in cell lysate of BMDMs. **c** The ratio of NAD^+ to NADH in BMDMs and J774A.1 macrophages primed with LPS and then treated with rhein or DMSO for 0.5 h and finally stimulated with ATP. **d** SPR assays on recombinant mouse SIRT2 incubated with rhein at the indicated concentrations. **e** MST assays on cell lysate of HEK-293T cells transfected with SIRT2-GFP incubated with rhein at the indicated concentrations. **f** Merge of the catalytic domain and highly flexible region of SIRT2 captured molecular dynamics simulations. **g** Keyframe of rhein-SIRT2 combination captured in molecular dynamics simulations. The dashed lines represent hydrogen bonds. Data are presented as the mean ± SD. Significance is indicated by $^*p < 0.05$ and $^{***}p < 0.001$ compared to the corresponding group. n.s. indicates no significance.

inhibitory effect of rhein on α-tubulin deacetylation along with NLRP3 inflammasome activation, which indicates that rhein treatment probably promotes the activity of SIRT2.

Considering that the activity of SIRT2 is nicotinamide adenine dinucleotide$^+$ (NAD^+)-dependent, we further measured the intracellular concentrations of NAD^+ and NADH[33]. However, rhein treatment changed neither the absolute value of NAD^+ nor the ratio of NAD^+ to NADH in macrophages (Fig. 6c; Fig. S5g, h), which means rhein does not affect the activity of SIRT2 by adjusting intracellular NAD^+ levels.

Excluding the impact of NAD^+, we supposed that rhein might regulate the activity of SIRT2 by directly binding to it. We next utilized the surface plasmon resonance (SPR) technique to detect the direct interaction between SIRT2 and rhein. After normalizing to the solvent (DMSO), rhein directly bound to the recombinant SIRT2 protein in a dose-dependent manner (the specific SIRT2 inhibitor AK-1 was used as a positive control) (Fig. 6d). Micro-scale thermophoresis (MST) measurement also verified the high affinity of rhein to SIRT2-EGFP with an estimated dissociation constant (KD) of 0.60 μM (Fig. 6e).

We further employed molecular dynamics simulations to investigate how the rhein-SIRT2 combination affects the conformation and the activity of SIRT2. A total simulation of 100 ns was conducted on the rhein-SIRT2 system with NAD^+. The root-mean-square-deviation (RMSD) curve showed that the rhein-SIRT2 system experienced two subtle disturbances (<0.05 nm) at 21.2 ns and 49.6 ns, then quickly equilibrated and finally stabilized at 0.4 nm (Fig. S6a). The radius of gyration (Rg) is an indicator of protein compactness. Consistent with RMSD, Rg fluctuated at 17.00 ns and 41.60 ns, which indicates a possible undergoing conformational changes of SIRT2 at these time points (Fig. S6c). The solvent-accessible surface area (SASA) of the

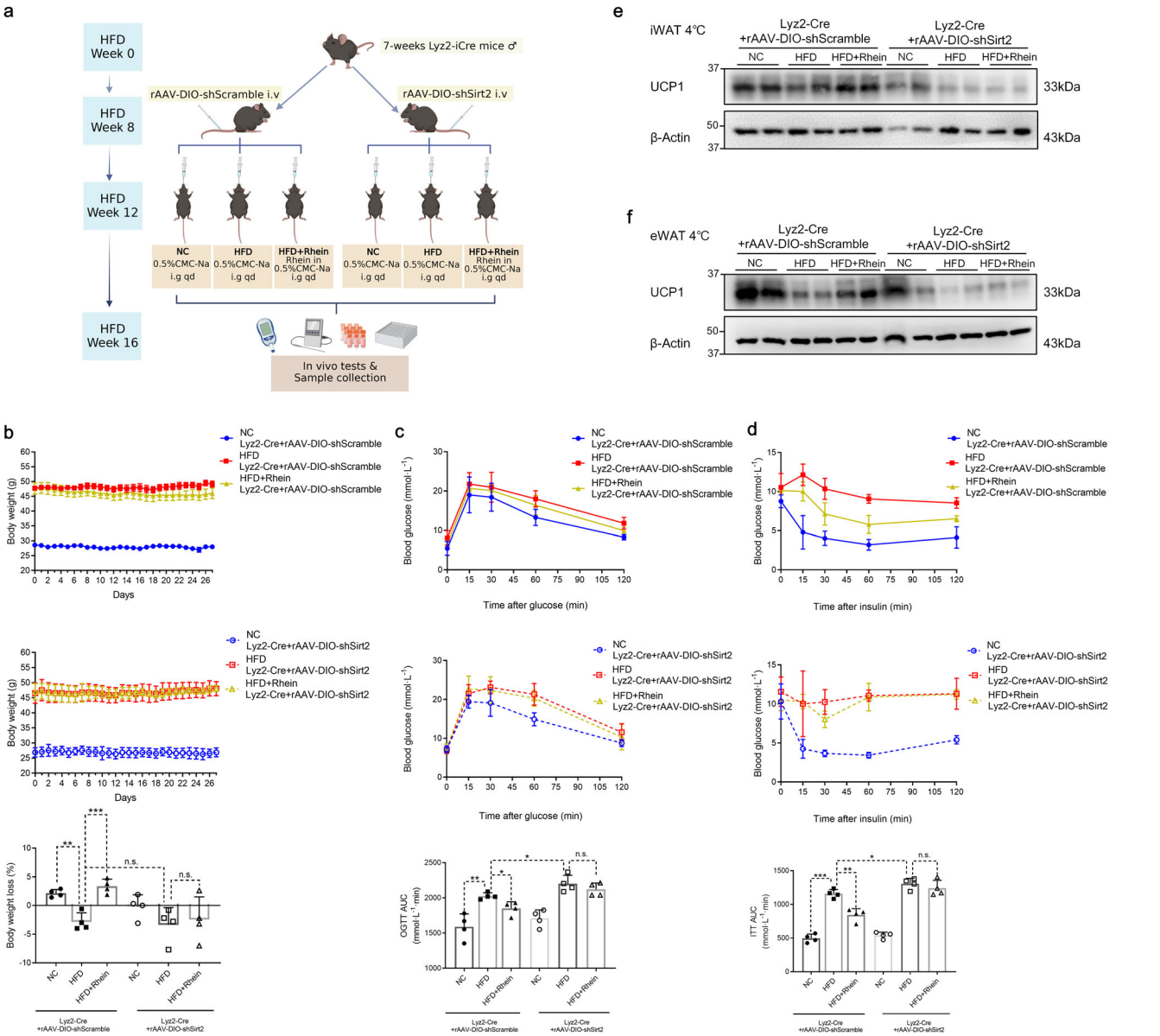

Fig. 7 | Selective *Sirt2* knockdown in myeloid cells impedes the metabolic-improving effect of rhein. a Workflow for the administration of rhein in myeloid *Sirt2*-knockdown mice. **b** Daily body weight of control and myeloid *Sirt2*-knockdown mice during rhein treatment ($n = 4$). **c** Oral glucose tolerance test on control and *Sirt2*-knockdown mice after a 12-h fast ($n = 4$). **d** i.p. insulin tolerance on control and *Sirt2*-knockdown mice after 6-h fast ($n = 4$). **e**, **f** Immunoblots of UCP1 in **e** iWAT and **f** eWAT in myeloid *Sirt2*-knockdown mice after 270-min cold exposure. Data are presented as the mean ± SD. Significance is indicated by $^{*}p < 0.05$, $^{**}p < 0.01$, and $^{***}p < 0.001$ compared to the corresponding group. n.s. indicates no significance.

system descanted smoothly (Fig. S6d), indicates the gradual tightening of the system. Root-mean-square-fluctuation (RMSF) was used to observe the conformation of local sites. Cut off at ±0.25 nm, the high flexible region captured in SIRT2 includes amino acids 53–56, 99–114, 198–199, 201–202, 295–304, 312–313, and 352–356 are right in the catalytic domain of SIRT2[34] (presented in red, Fig. 6f). The key frame of rhein-SIRT2 is shown in Fig. 6g. Until the end of the simulation, the number of hydrogen bonds in the system had significantly increased (Fig. S6e). These results all support that the rhein-SIRT2 combination alters the conformation of the catalytic domain of SIRT2, which explains the promotion of SIRT2 catalytic activity by rhein.

Macrophage SIRT2 is required for rhein-induced WAT thermogenesis

To investigate whether the beneficial effect of rhein on metabolism depends on SIRT2 in macrophages, we ablated *Sirt2* expression in myeloid cells by caudal vein injection of adeno-associated virus expressing double-floxed inverse orientation-*Sirt2* short hairpin RNA (rAAV-DIO-shSirt2) to *Lyz2*-iCre mice and then administered these mice with rhein (Fig. 7a). Compared with the scrambled control, rAAV-DIO-sh*Sirt2* injection significantly down-regulated *Sirt2* expression in the SVFs isolated from iWAT and eWAT (Fig. S7a, b). As shown in Fig. 7b, though myeloid *Sirt2* knockdown (KD) did not affect the body weight of both the NC and the HFD mice significantly, rhein treatment failed to reduce the gain of body weight in the mice with selective *Sirt2* KD in myeloid cells. Inconsistent with the change of body weight, the myeloid *Sirt2* KD mice presented impaired glucose as well as insulin tolerance compared to the scrambled controls under the condition of HFD (Fig. 7c, d). However, the improving effects of rhein on glucose and insulin tolerance were still blunted in the myeloid *Sirt2* KD mice (Fig. 7c, d). Myeloid *Sirt2* KD also blunts the effect of rhein on reducing circulating NEFA (Fig. S7c).

We further examined the state of adipose tissue thermogenesis in the myeloid *Sirt2* KD mice with or without rhein treatment. The rectal temperature of the mice with selective *Sirt2* KD in myeloid cells showed no difference among the NC, HFD, and HFD + Rhe groups, regardless of whether at room temperature or under cold stimulation (Fig. S7d, e). Compatible with our previous findings, rhein treatment significantly upregulated UCP1 abundance in both iWAT and eWAT of scrambled controls fed with HFD but failed to do so in neither iWAT nor eWAT of the myeloid *Sirt2* KD mice (Fig. 7e, f; Fig. S7f, g). These results confirm the essential role of macrophage SIRT2 in rhein-mediated white adipose tissue thermogenesis and the related improvement of metabolism.

In summary, our data demonstrate that rhein inhibits NLRP3 inflammasome activation by promoting SIRT2 activity in macrophages, and thus improves adipose tissue thermogenesis in the context of obesity (Fig. 8).

Discussion

Broadly, adipocytes are divided into either white or brown. White adipocytes are demarcated by large unilocular lipid droplets with relatively few mitochondria and are commonly regarded as the classic 'energy warehouse' of the body. Brown adipocytes possess high-density mitochondria as well as small multilocular lipid droplets, dissipating energy in the form of heat through abundant UCP1 on the inner mitochondrial membrane[25]. Adipocytes typically reside in different depots known as brown adipose tissue and white adipose tissue. Various stimuli, including adrenergic activation and cold exposure, induce the generation of a subset of adipocytes residing in WAT with similar morphology and thermogenesis function to brown adipocytes named beige adipocyte[35]. Compared with BAT thermogenesis, the beginning of WAT represents a more appealing concept for combating obesity, for BAT may not even exist in adult patients with obesity[36]. Herein, we demonstrated that rhein elevates the thermogenesis capacity of both visceral and subcutaneous white adipose tissue in DIO mice, and thus improves the metabolic disorders induced by obesity. Our data indicate the potential of rhein in mitigating obesity and its related metabolic disorders.

Though monumental progress in the development of medications promoting adipose tissue thermogenesis has been achieved, rare of them are now truly used in clinical practice, for adipose thermogenesis is not always beneficial[37]. In cancer cachexia, burn injuries, sepsis, and drug-induced malignant hyperthermia, it is widely accepted that persistently active adipose tissue thermogenesis and the accompanying hyperthermia, as well as the hyper-catabolic condition, are vital contributors to insulin resistance, ectopic lipid deposition, arrhythmia and even death[38]. On the other hand, while mirabegron, a β3-adrenergic receptor agonist, has been proven to be adipose tissue thermogenesis-promoting and insulin sensitivity-improving in young healthy adults, researchers are paying boosting attention to the possible cardiovascular detrimental effects of adrenergic receptor agonizts in the patients with metabolic diseases and elderly patients, especially in the context that dose of mirabegron required to promote adipose tissue thermogenesis (100 mg qd) is much higher than the recommended dose approved by the FDA for the treatment of overactive bladder[39]. Therefore, effective as well as safe strategies for promoting adipose tissue thermogenesis are still unexplored. Here, we showed that rhein promotes WAT thermogenesis by inhibiting the activation of NLRP3 inflammasome in macrophages, and thus mitigates the metabolic disorders induced by obesity. Rhein's effect on promoting thermogenesis by reducing metabolic inflammation, to a certain extent, avoids the possible cardiovascular adverse events and the risks brought by unlimited thermogenesis, which makes rhein a promising drug to treat obesity via promoting thermogenesis.

In this study, we also confirmed that rhein directly binds to the SIRT2 protein and inhibits the activation of NLRP3 inflammasome in a SIRT2 activity-dependent way. As a member of the KDACs, SIRT2 was proven to suppress NLRP3 inflammasome activation through deacetylating NLRP3 and α-tubulin[32,40]. But, the acetylation of both NLRP3 and α-tubulin was not captured by LC/MS–MS. It is worth noting that although LC/MS-MS is widely used for high-throughput detection of PTMs, information on modifications may be lost due to the limitations of cleavage sites of trypsin. Thus, immunoblots with antibodies targeted to specific acetylated lysine remain the most accurate way to detect the specific acetylation of a protein currently. In this study, after targeting SIRT2 as the drug target, we detected the acetylation of α-tubulin using an anti-α-tubulin (acetyl lys40) antibody and identified that rhein reduces the acetylation of α-tubulin induced by LPS + ATP in a SIRT2-dependent way as well. However, we failed to detect the acetylation of NLRP3 in NLRP3-activated J774A.1 macrophages (Fig. S5f), possibly due to the differences in cell type and experimental condition (glucose starvation was not employed in our research). Nevertheless, this does not matter our conclusion. Moreover, we screened out 25 proteins related to inflammasome components from quantitative acetylome analysis. Their acetylation could be regulated by rhein and is associated with a variety of biological processes (Fig. 5e, f; Fig. S4a–d). We took the interactions between these 25 proteins and acetylation-modifying enzymes as a clue and identified SIRT2 as the drug target of rhein. Yet, there is still a lack of reports on the relationship between the acetylation of some of these proteins and the activation of NLRP3 inflammasome, which deserves further exploration.

SIRT2 exists in multiple types of cells, and rhein may interact with SIRT2 in all these cells theoretically. However, our study demonstrates that rhein regulates SIRT2 predominantly in macrophages at clinically relevant doses, because the knockdown of *Sirt2* selectively in myeloid cells abrogates the beneficial effects on metabolism of rhein in DIO mice. It has been reported that SIRT2 regulates adipocyte differentiation and lipolysis in adipocytes[41,42]. Thus, we cannot exclude the possibility that higher doses of rhein may target SIRT2 in adipocytes directly to affect metabolism. On the other hand, the diversity of SIRT2's catalytic substrates may be the basis for the wide range of rhein's pharmacological actions. For example, it was reported that rhein treatment directly downregulates the expression of peroxisome proliferator-activated receptor-γ (PPAR-γ) in 3T3-L1 preadipocytes and thus impairs adipocyte differentiation[19]. Meanwhile, SIRT2 has also been proven to suppress PPAR-γ expression in adipocytes through deacetylating FOXO1[42,43]. Similarly, the inhibitory effect of long-time rhein treatment on NF-κB activation may rely on SIRT2-catalyzed acetylation of NF-κB p65 subunit[44]. Moreover, Sheng et al. reported that high doses of rhein failed to neither reduce the body weight nor increase UCP1 expression in brown adipose tissue in DIO mice with liver X receptor (LXR) knockout, and they speculated that might be caused by rhein-LXR interaction[7,20]. However, recent studies also confirmed that SIRT2 knockdown also significantly inhibits the PPARs/LXRα pathway in bovine ovarian granular cells[45]. Taken together, the evidence above reminds us that diverse pharmacological properties of rhein may be explained by the action of SIRT2, and rhein may be introduced into the wide application for more disorders by regulating SIRT2.

However, there are still several limitations in this study. Firstly, while we observed that rhein promotes UCP1 expression in an NE-dependent way in the co-culture system, we were unable to get the accurate quantity of NE directly using HLPC either in culture supernatant or adipose tissue due to the extremely short half-life of NE. Secondly, due to the restriction of the transwell co-culture system, we were unable to perform seahorse analysis on adipocytes to measure the condition of proton leak directly. Finally, because of the strong reducibility and spontaneous fluorescence of rhein, existing commercial SIRT2 activity detection kits are not appropriate to be employed to evaluate the impact of rhein on SIRT2 activity.

In conclusion, our results elucidate that rhein promotes white adipose tissue thermogenesis by inhibiting the activation of NLRP3 inflammasome in macrophages during obesity. Furthermore, we reveal that rhein directly binds to SIRT2 protein and inhibits the activation of NLRP3 inflammasome in a SIRT2 activity-dependent manner. These findings uncover the molecular mechanism underlying the beneficial effect of rhein on metabolism, suggesting that rhein may become a potential drug for treating obesity.

Methods

Reagents and materials

The materials and reagents used in this article are listed in Supplementary Data 1.

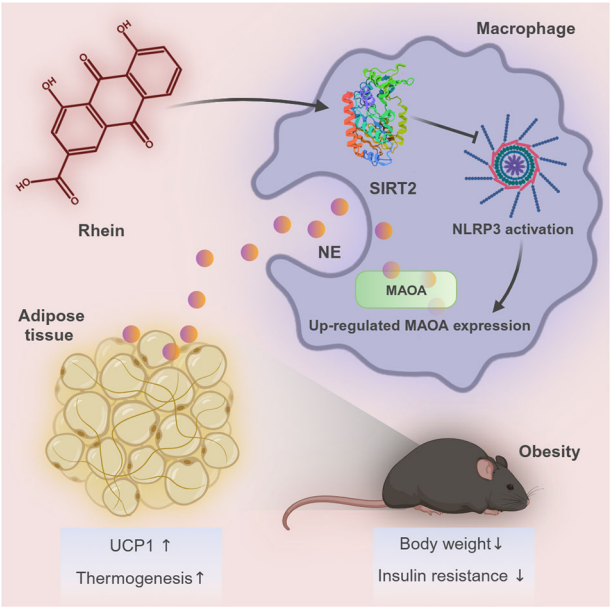

Fig. 8 | Graph summary. During obesity, rhein promotes adipose tissue thermogenesis by suppressing the activation of NLRP3 inflammasome in adipose tissue-resident macrophages. Furthermore, SIRT2 is a direct molecular target of rhein, and rhein inhibits the activation of NLRP3 inflammasome and promotes adipose tissue thermogenesis in a macrophage SIRT2-dependent manner.

Mouse models

The animal experiments were conducted in accordance with the provision and general recommendation of Chinese experimental animal administration legislation, and the detailed protocols were approved by the ethics committee of Nanjing University of Chinese Medicine (permit number: 202010A033). Six-week-old C57BL/6 J male mice (SPF grade) were purchased from SLAC Company (Shanghai, China), and 6-week-old C57BL/6JGpt-*Lyz2*$^{em1Cin(iCre)}$/Gpt male mice (SPF grade) were purchased from GemPharmatech Company (Nanjing, China). The animals were kept under an environment of 22 ± 2 °C, 12-h light–dark cycles, and relative humidity of 50 ± 15%. Sterile water was given *ad libitum* during the whole experiment. We have complied with all relevant ethical regulations for animal use.

C57BL/6 J male mice were randomly divided into 2 groups following 1-week acclimatization after importing into the facility. A standard normal chow diet (NC, Research Diet, Cat# D12450J) and a high-fat diet (HFD, Research Diet, Cat# D12492) were provided to the corresponding group for 12 weeks to generate DIO models. DIO mice were further divided into the HFD group and the HFD + Rhein group randomly, and given 10 mg/kg rhein or solvent (0.05% CMC-Na) with a corresponding volume per day by gavage for 28 days. Body weight was measured daily.

Similarly, C57BL/6JGpt-*Lyz2*$^{em1Cin(iCre)}$/Gpt male mice were given NC or HFD following 1-week acclimatization. At the end of the 8th week of DIO modeling, NC and HFD mice were randomly divided into 2 groups separately and injected with rAAV-DIO-sh*Scramble* or rAAV-DIO-sh*Sirt2* via tail vein and continuously given NC or HFD for 4 weeks to finish the 12-week DIO modeling before 28-day rhein treatment.

Cell culture

3T3-L1 cells were maintained in Dulbecco's modified eagle medium (DMEM) with 10% fetal bovine serum (FBS). Upon meeting complete confluence, the cells were induced to mature adipocytes by 2-day treatment of induction A (DMEM with 10% FBS with 0.5 mM 3-isobutyl-1-methylxanthine, 1 μM dexamethasone and 1.67 μM insulin) followed by 2-day treatment of induction B (DMEM with 10% FBS with 1.67 μM insulin) and 2-day treatment of DMEM with 10% FBS. J774A.1 cells were maintained in DMEM with 10% FBS, and 3 to 10 passages of J774A.1 cells were used to conduct the experiments. Mouse primary white adipocytes differentiated from SVFs of iWAT isolated from newborn (3–7 day old) C57BL/6 J mice. Post-confluent cells were induced to mature white adipocytes by 2-day treatment of induction A (DMEM with 10% FBS with 0.5 mM 3-isobuthyl-1-methylxantine, 1 μM dexamethasone and 170 nM insulin) followed by 2-day treatment of induction B (DMEM with 10% FBS with 170 nM insulin). Bone marrow-derived macrophages were isolated from 6-week-old C57BL/6 J male mice and induced to be mature by macrophage colony-stimulating factor (M-CSF)[2].

Calculations for clinically relevant doses of rhein

According to the recommended dosage of diacerein clinically (100 mg/day = 0.272 mol/day), the dosage of rhein recommended for humans is 77.17 mg/day. The conversion of human doses to animal equivalent doses is recommended to conduct based on body surface area. The clinically relevant dose of rhein in mice = 77.17 mg/day × 0.0026 (the conversion factor) ÷ 0.02 kg (assumes 0.02 kg mouse) = 10.03 mg/kg per day. We finally took the concentration of 10.00 mg/kg per day for the advantage of operation.

Metabolic cages

Energy expenditure, food intake, drink consumption and physical activities of mice were determined with TSE phenomaster animal monitoring system (TSE, Germany). The mice were acclimated to the system for 48 h before formal testing with free access to food and water. The data of whole-body energy expenditure was normalized with body weight.

Cold exposure test

After 12 h of fast, mice were stored in a cold room (4–8 °C) to test their cold tolerance, and the mice had free access to water during this period. Rectal temperatures were measured at 0, 30, 60, 90, 120 and 270 min using a digital thermometer (TH212, China) to represent the core body temperature.

GTTs and ITTs

In glucose tolerance tests (GTTs), mice were administered 2.5 g/kg of glucose solution by gavage after a 12-h fast. In insulin tolerance tests (ITTs), 0.75 IU/kg of insulin (WanBang, China) was intraperitoneally injected into mice after a 6-hour fast. Blood glucose was monitored by pricking the tail at the time points of 0, 15, 30, 60, 90 and 120 min with a glucometer.

Macrophage preparation and stimulation

To observe the influences of rhein on NLRP3 inflammasome activation in BMDMs, the cells were primed with 100 ng/mL LPS for 12 h and then treated with rhein or solvent (DMSO) for 0.5 h and finally stimulated with 3 mM ATP for 30 min or 1.5 mM nigericin for 1 h or 0.5 g/L MSU for 4 h. In J774A.1 cells, the second stimulation was 4 mM ATP for 30 min. siRNAs were purchased from GenePharma Company (Shanghai, China) and were transfected into J774A.1 cell via RNAiMax priming according to the manufacturer's instructions 48–60 h prior to LPS (si-RNA sequences are listed in Table S1).

Adipocyte preparation and stimulation

Mature white adipocytes induced from mice SVFs or 3T3-L1 pre-adipocytes were starved with DMEM with 0.2% bovine serum albumin (BSA) for 24 h prior to use. In Fig. 4B, C, adipocytes were treated with NE gradient for 1 h before mRNA sample collection.

Construction of macrophage-adipocyte co-culture system

As illustrated in Fig. 4A, BMDMs were seeded and induced in the culture inserts (Transwell permeable supports, 0.4μm polyester membrane, Coring) while mouse SVFs or 3T3-L1 pre-adipocytes were seeded and induced in the corresponding well plates. BMDMs and mature white adipocytes induced from mouse SVFs or 3T3-L1 pre-adipocytes were prepared as described above. Upon adding ATP to the culture inserts, adipocytes were stimulated with NE simultaneously, and culture inserts were quickly put into adipocyte culture plates for the 1-hour co-culture.

Micro-CT scan and analysis
Mice were anesthetized with isoflurane and scanned by Quantum GX micro-CT imaging system (PerkinElmer, US), and the data were analyzed with Analyze 12.0 (PerkinElmer, US).

NEFA analysis
Serum NEFA levels of mice were tested by biochemical examination kits (Wako, Japan) according to the manufacturer's instructions.

Viability assay
BMDMs and J774A.1 cells were seeded in 96-well plates for 24 h before being treated with rhein gradient or DMSO for another 24 h. The cell counting kit-8 (CCK8) assay was employed for cell viability estimation according to the manufacturer's instructions for the CCK8 kit (Dojindo, Japan).

qRT-PCR
Total RNA was prepared from a tissue or cell sample with a total RNA extraction reagent (Vazyme, Nanjing) following the manufacturer's instructions. cDNA was generated using PrimerScript RT reagent Kit (Vazyme, Nanjing). qRT-PCR was performed on the 7500 Real-Time PCR System (Applied Biosystems, US) using ChamQ SYBR qPCR Master Mix (Vazyme, Nanjing). Primers used for qRT-PCR are listed in Table S1.

ELISA
The culture supernatant of macrophages was collected and centrifuged at 300*g* for 10 min to remove the pellets. The following steps were performed according to the manufacturer's instructions. The IL-1β concentration was tested by a mouse IL-1β valukine ELISA kit (Novus, US) or mouse IL-1β ELISA kit (MutiSciences, China). The IL-1β concentration was tested by a mouse TNF-α ELISA kit (MutiSciences, China).

Immunoprecipitation and immunoblotting
For immunoblots of cell culture supernatant, trichloroacetic acid was used to precipitate the proteins from the culture supernatant, and the pellets were resuspended in the loading buffer. Immunoprecipitation and immunoblotting analysis were performed following a standard protocol[2]. The dilution of each antibody are described in Supplementary Data 1.

Immunofluorescence
BMDMs were seeded and treated as described in CellCarrier-96 black plates (PerkinElmer, US). 4% paraformaldehyde was used to fix the cells, followed by 0.1% Triton treatment and 5% BSA block. Immunofluorescence staining was conducted according to the standard protocols of the antibodies. Finally, Operetta High content screening (HSC) system (PerkinElmer, US) was employed for image capture and analysis.

TMRE staining
Adipocytes were stained with 1 μM pre-warmed TMRE dye (MedChemExpress, US) for 15 min after the co-culture. Cell images were captured by the fluorescence microscope (Leica, Germany), and the fluorescence intensity was measured by the microplate reader (PerkinElmer, US).

PI staining
Macrophages were stained with 20 μM pre-warmed PI solution for 10 min after ATP stimulation. For flowcytometry, cells from the supernatant were also collected and stained with PI. Cell images were captured by the fluorescence microscope (Leica, Germany), and flowcytometry was conducted with the flowcytometer (BeckmanCoulter, US).

Micro-scale thermophoresis (MST) assay
Plasmid encoding SIRT2-EGFP was transfected into HEK-293T cells 3 days prior to the MST analysis. RIPA buffer (Millipore, US) with protease inhibitor was used to acquire the cell lysate, and the protein concentration was measured by the BCA assay (Thermofisher, US). Rhein was diluted to a gradient, and the runs were conducted and the data were analyzed following the manufacturer's instruction of Monolith (NanoTemper, Germany).

Surface plasmon resonance (SPR) assay
Experiments were performed at 25 °C on the Reichert 4 SPR (Reichert, US) using the SR7000 gold sensor slide. Briefly, the sensor slide was activated by carbodiimide and N-hydroxysuccinimide, and human recombinant SIRT2 protein (CaymanChemical, US) was diluted in acetate solution pH 4.0 and immobilized on the surface of one channel of the sensor with a neighboring channel serving as a reference. The channels were blocked with 1 M ethanolamine. Rhein was diluted to a gradient, and the runs were conducted following the manufacturer's instructions. Finally, the data were analyzed using Trace Drawer software (Reichert, US).

Acetylome analysis
The acetylome analysis was performed by PTM-Biolabs (Hangzhou, China). Briefly, the cell lysate was digested twice with trypsin at 1:50 trypsin-to-protein mass ratio and 1:100 trypsin-to-protein mass ratio respectively, and the peptides were further desalted by C18 SPE column. To enrich modified peptides, the pre-washed antibody beads (PTM Bio, Cat# PTM-104) were incubated with tryptic peptides (dissolved in NETN buffer) at 4 °C overnight, and then 0.1% trifluoroacetic acid was used to elute the bound peptide from the beads. Finally, the eluted fractions were combined, vacuum-dried, desalted, and resuspended for the LC-MS analysis. The results were analyzed with the MaxQuant search engine (v.1.6.15.0). The screening of differential modification sites followed the criteria of $p < 0.05$ with a fold change > 1.5 or <0.67. The NLRP3 inflammasome components-related proteins and the protein-protein connections were identified using the STRING database (active interaction sources: textmining, experiments, databases, co-expression; minimum required interaction score: 0.180). Gene Ontology (GO) annotation was derived from the UniProt-GOA database. Wolfpsort was used for the predication of protein subcellular localization. The Kyoto Encyclopedia of Genes and Genomes (KEGG) database was used to annotate protein pathways.

Molecular dynamics simulations
The SIRT2 protein sequence was acquired from UniProt (Q8VDQ8), and the parts with low modeling quality at the N-terminal (residue 1–51) and C-terminal (367–389) were removed, and the removed regions are not in the protein function domain of SIRT2[34]. Rhein structure was obtained from PubChem (10168). Structural optimization and charge calculation were carried out using Orca under B3LYP/ 6–31 G* conditions[46]. The semi-flexible docking of SIRT2 and rhein was performed by Smina[47,48]. The docking box was set to completely envelop SIRT2, and the exhaustiveness was set at 20. Molecular dynamics simulations were run by GROMACS 2019.6[49]. The protonation states of proteins were determined by the PROPKA3[50]. The initial conformation for molecular dynamics simulations was the result of docking. Amber14sb was chosen as the protein force field[51]. The GaFF2 was chosen as the force field for NAD^+ and Rhein[52]. The TIP3P water model was adopted to establish the water box (with the edge of the water box at least 1.2 nm away from the protein edge), and Na^+/Cl^- was added to balance the system (0.15 mol/L). The cut-off of Coulomb force and Van der Waals radius were both set to 1.4 nm. Particle-mesh Ewald (PME) was used to treat electrostatic interactions within 0.16 nm, and the steepest descent method was used to minimize energy with the maximum number of steps (50,000 steps). Finally, the molecular dynamics simulations were run for 100 ns in total, and the energy and position coordinates were recorded every 20 ps. The structure of the wild-type SIRT2 with NAD^+ was obtained by a 50 ns molecular dynamics simulation. The time step of molecular dynamics simulations was 2 fs. The cutoff of non-bond interaction was set to 10 Å. The simulation temperature was controlled to 300 K using the V-rescale temperature coupling method, and the pressure was controlled to 1 bar using the Berendsen method.

Statistics and reproducibility

Statistical analysis was performed using Prism 9.0 (GraphPad, US). A comparison between 2 groups was conducted by Student's *t* test or Welch's *t* test based on the homogeneity of variance. Comparison among groups of more than 2 was performed using a one-way analysis of variance (ANOVA) followed by Tukey's test. Data are presented as the mean ± standard error (SD). Significance is indicated by $^{*}p < 0.05$, $^{**}p < 0.01$, $^{***}p < 0.001$ compared to the corresponding group. n.s. indicates no significance. The numbers of repetitions are shown in the corresponding legends, and a biologically independent sample was employed for each repetition.

Reporting summary

Further information on research design is available in the Nature Portfolio Reporting Summary linked to this article.

Data availability

The raw data of the acetylome has been deposited to the ProteomeXchange Consortium via the PRIDE partner repository with the identifier PXD044992. Uncropped and unedited blot images are shown in Figs. S8–14. The files of the initial coordinate, simulation input, and the protonation state from the molecular dynamics simulations are uploaded as Supplementary Data 2. Source data for charts and graphs can be found in Supplementary Data 3. The publication license of figures created using Biorender is uploaded as Supplementary Data 4. Additional data are available from the corresponding author upon request.

Received: 22 January 2024; Accepted: 6 August 2024;
Published online: 16 August 2024

References

1. Hotamisligil, G. S. Inflammation, metaflammation and immunometabolic disorders. *Nature* **542**, 177–185 (2017).
2. Zhang, S. et al. Acetylation of p65Lys310 by p300 in macrophages mediates anti-inflammatory property of berberine. *Redox Biol.* **62**, 102704 (2023).
3. Sakers, A., De Siqueira, M. K., Seale, P. & Villanueva, C. J. Adipose-tissue plasticity in health and disease. *Cell* **185**, 419–446 (2022).
4. Xiang, H., Zuo, J., Guo, F. & Dong, D. What we already know about rhubarb: a comprehensive review. *Chin. Med.* **15**, 88 (2020).
5. Spencer, C. M. & Wilde, M. I. Diacerein. *Drugs* https://doi.org/10.2165/00003495-199753010-00007 (1997)
6. Wang, S. et al. Chronic rhein treatment improves recognition memory in high-fat diet-induced obese male mice. *J. Nutr. Biochem.* **36**, 42–50 (2016).
7. Sheng, X. et al. Rhein ameliorates fatty liver disease through negative energy balance, hepatic lipogenic regulation, and immunomodulation in diet-induced obese mice. *Am. J. Physiol. Endocrinol. Metab.* **300**, E886–E893 (2011).
8. Ji, L. & Gu, H. The anti-obesity effects of rhein on improving insulin resistance (IR) and blood lipid levels are involved in endoplasmic reticulum stress (ERs), inflammation, and oxidative stress in vivo and vitro. *Bioengineered* **12**, 5797–5813 (2021).
9. Almezgagi, M. et al. Diacerein: Recent insight into pharmacological activities and molecular pathways. *Biomed. Pharmacother.* **131**, 110594 (2020).
10. He, Y., Hara, H. & Núñez, G. Mechanism and regulation of NLRP3 inflammasome activation. *Trends Biochem. Sci.* **41**, 1012–1021 (2016).
11. Ge, H. et al. Rhein attenuates inflammation through inhibition of NF-κB and NALP3 inflammasome in vivo and in vitro. *Drug Des. Dev. Ther.* **11**, 1663–1671 (2017).
12. Shen, C. et al. Rhein suppresses lung inflammatory injury induced by human respiratory syncytial virus through inhibiting NLRP3 inflammasome activation via NF-κB pathway in mice. *Front. Pharm.* **10**, 1600 (2019).
13. Zhou, Y. et al. Rhein regulates redox-mediated activation of NLRP3 inflammasomes in intestinal inflammation through macrophage-activated crosstalk. *Br. J. Pharmacol.* **179**, 1978–1997 (2022).
14. Wu, C. et al. Rhubarb free anthraquinones improved mice nonalcoholic fatty liver disease by inhibiting NLRP3 inflammasome. *J. Transl. Med*. **20**, 294 (2022).
15. Yao, J., Wu, D. & Qiu, Y. Adipose tissue macrophage in obesity-associated metabolic diseases. *Front. Immunol.* **13**, 977485 (2022).
16. Wang, X., Wang, Y., Antony, V., Sun, H. & Liang, G. Metabolism-associated molecular patterns (MAMPs). *Trends Endocrinol. Metab.* **31**, 712–724 (2020).
17. Camell, C. D. et al. Inflammasome-driven catecholamine catabolism in macrophages blunts lipolysis during ageing. *Nature* **550**, 119–123 (2017).
18. Du, H. et al. Improvement of glucose tolerance by rhein with restored early-phase insulin secretion in db/db mice. *J. Endocrinol. Invest.* **35**, 607–612 (2012).
19. Zhang, Y. et al. Rhein reduces fat weight in db/db mouse and prevents diet-induced obesity in C57Bl/6 Mouse through the Inhibition of PPARγ Signaling. *PPAR Res.* **2012**, 374936 (2012).
20. Sheng, X. et al. Rhein protects against obesity and related metabolic disorders through liver X receptor-mediated uncoupling protein 1 upregulation in brown adipose tissue. *Int. J. Biol. Sci.* **8**, 1375–1384 (2012).
21. Nicolas, P., Tod, M., Padoin, C. & Petitjean, O. Clinical pharmacokinetics of diacerein. *Clin. Pharmacokinet.* **35**, 347–359 (1998).
22. Kahn, S. E., Hull, R. L. & Utzschneider, K. M. Mechanisms linking obesity to insulin resistance and type 2 diabetes. *Nature* **444**, 840–846 (2006).
23. Carpentier, A. C. 100th anniversary of the discovery of insulin perspective: insulin and adipose tissue fatty acid metabolism. *Am. J. Physiol. Endocrinol. Metab.* **320**, E653–E670 (2021).
24. Chassany, O., Michaux, A. & Bergmann, J. F. Drug-induced diarrhoea. *Drug Saf.* **22**, 53–72 (2000).
25. Chouchani, E. T., Kazak, L. & Spiegelman, B. M. New Advances in Adaptive Thermogenesis: UCP1 and Beyond. *Cell Metab.* **29**, 27–37 (2019).
26. Fromme, T. & Klingenspor, M. Uncoupling protein 1 expression and high-fat diets. *Am. J. Physiol. Regul. Integr. Comp. Physiol.* **300**, R1–R8 (2011).
27. Jones, S. A., Ruprecht, J. J., Crichton, P. G. & Kunji, E. R. S. Structural mechanisms of mitochondrial uncoupling protein 1 regulation in thermogenesis. *Trends Biochem Sci*. https://doi.org/10.1016/j.tibs.2024.03.005 (2024)
28. Swanson, K. V., Deng, M. & Ting, J. P. Y. The NLRP3 inflammasome: molecular activation and regulation to therapeutics. *Nat. Rev. Immunol.* **19**, 477–489 (2019).
29. Xia, J., Jiang, S., Dong, S., Liao, Y. & Zhou, Y. The Role of Post-Translational Modifications in Regulation of NLRP3 Inflammasome Activation. *Int J Mol Sci* **24**. https://doi.org/10.3390/ijms24076126 (2023)
30. Li, P., Ge, J. & Li, H. Lysine acetyltransferases and lysine deacetylases as targets for cardiovascular disease. *Nat Rev Cardiol* **17**. https://doi.org/10.1038/s41569-019-0235-9 (2020)
31. Magupalli, V. G. et al. HDAC6 mediates an aggresome-like mechanism for NLRP3 and pyrin inflammasome activation. *Science* **369**, eaas8995 (2020).
32. Misawa, T. et al. Microtubule-driven spatial arrangement of mitochondria promotes activation of the NLRP3 inflammasome. *Nat. Immunol.* **14**, 454–460 (2013).
33. Wang, Y., Yang, J., Hong, T., Chen, X. & Cui, L. SIRT2: Controversy and multiple roles in disease and physiology. *Ageing Res. Rev.* **55**, 100961 (2019).
34. Finnin, M. S., Donigian, J. R. & Pavletich, N. P. Structure of the histone deacetylase SIRT2. *Nat. Struct. Biol.* **8**, 621–625 (2001).

35. Sidossis, L. & Kajimura, S. Brown and beige fat in humans: thermogenic adipocytes that control energy and glucose homeostasis. *J. Clin. Invest* **125**, 478–486 (2015).
36. Wibmer, A. G. et al. Brown adipose tissue is associated with healthier body fat distribution and metabolic benefits independent of regional adiposity. *Cell Rep. Med.* **2**, 100332 (2021).
37. Stohs, S. J. & Badmaev, V. A Review of Natural Stimulant and Non-stimulant Thermogenic Agents. *Phytother. Res.* **30**, 732–740 (2016).
38. Auger, C. & Kajimura, S. Adipose Tissue Remodeling in Pathophysiology. *Annu Rev. Pathol.* **18**, 71–93 (2023).
39. O'Mara, A. E. et al. Chronic mirabegron treatment increases human brown fat, HDL cholesterol, and insulin sensitivity. *J. Clin. Invest* **130**, 2209–2219 (2020).
40. He, M. et al. An acetylation switch of the NLRP3 inflammasome regulates aging-associated chronic inflammation and insulin resistance. *Cell Metab.* **31**, 580–591 (2020).
41. Krishnan, J. et al. Dietary obesity-associated Hif1α activation in adipocytes restricts fatty acid oxidation and energy expenditure via suppression of the Sirt2-NAD+ system. *Genes Dev.* **26**, 259–270 (2012).
42. Jing, E., Gesta, S. & Kahn, C. R. SIRT2 regulates adipocyte differentiation through FoxO1 acetylation/deacetylation. *Cell Metab.* **6**, 105–114 (2007).
43. Wang, F. & Tong, Q. SIRT2 suppresses adipocyte differentiation by deacetylating FOXO1 and enhancing FOXO1's repressive interaction with PPARgamma. *Mol. Biol. Cell* **20**, 801–808 (2009).
44. Rothgiesser, K. M., Erener, S., Waibel, S., Lüscher, B. & Hottiger, M. O. SIRT2 regulates NF-κB dependent gene expression through deacetylation of p65 Lys310. *J. Cell Sci.* **123**, 4251–4258 (2010).
45. Xu, D. et al. SIRT2 plays a novel role on progesterone, estradiol and testosterone synthesis via PPARs/LXRα pathways in bovine ovarian granular cells. *J. Steroid Biochem Mol. Biol.* **185**, 27–38 (2019).
46. Neese, F., Wennmohs, F., Becker, U. & Riplinger, C. The ORCA quantum chemistry program package. *The Journal of Chemical Physics* **152**. https://doi.org/10.1063/5.0004608 (2020)
47. Koes, D. R., Baumgartner, M. P. & Camacho, C. J. Lessons learned in empirical scoring with smina from the CSAR 2011 benchmarking exercise. *J. Chem. Inf. Model* **53**, 1893–1904 (2013).
48. Cui, Z. et al. Noteworthy Consensus Effects of D/E Residues in Umami Peptides Used for Designing the Novel Umami Peptides. *J. Agric Food Chem.* **72**, 2789–2800 (2024).
49. Spoel, D. V. D., Lindahl, E., Hess, B., Groenhof, G. & Berendsen, H. GROMACS: fast, flexible, and free. *J. Comput Chem.* **26**, 1701–1718 (2005).
50. Olsson, M. H. M., Søndergaard, C. R., Rostkowski, M. & Jensen, J. H. PROPKA3: Consistent Treatment of Internal and Surface Residues in Empirical pKa Predictions. *J. Chem. Theory Comput* **7**, 525–537 (2011).
51. Huai, Z., Shen, Z. & Sun, Z. Binding Thermodynamics and Interaction Patterns of Inhibitor-Major Urinary Protein-I Binding from Extensive Free-Energy Calculations: Benchmarking AMBER Force Fields. *J. Chem. Inf. Model* **61**, 284–297 (2021).
52. Sprenger, K. G., Jaeger, V. W. & Pfaendtner, J. The general AMBER force field (GAFF) can accurately predict thermodynamic and transport properties of many ionic liquids. *J. Phys. Chem. B* **119**, 5882–5895 (2015).

Acknowledgements

This study was supported by the National Natural Science Foundation of China (81873060, 81473391, and 82374100), the Priority Academic Program Development of Jiangsu Higher Education Institutions (ZYX03KF058), and the Graduate Research and Innovation Projects of Jiangsu Province (KYCX23_2133 and SJCX23_0728). We express our sincere gratitude to Dr. Zhiyong Cui from Shanghai Jiaotong University for assisting us with molecular dynamics simulations.

Author contributions

Ruonan Zhou was involved in experimental design and most procedures, data acquisition, and analyses in cells and animal experiments and writing the paper. Ziwei Zhu and Pingyuan Xu assisted in the performance of cell experiments. Lixuan Shen, Ziwei Wang, Yingying Xue, Yingying Xiang, Yue Cao, Xizhong Yu, and Jing Yan assisted in the performance of animal experiments. Juan Zhao and Yu Jin contributed to the performance of the immunofluorescence experiment. Qin Yang helped in the revision and edition of this paper. Penghua Fang and Wenbin Shang contributed to the design of the study and the writing of this paper. Wenbin Shang supervised this work, had full access to all the data in the study, and took responsibility for the integrity of the data and the accuracy of the data analysis.

Competing interests

The authors declare no competing interests.

Additional information

Supplementary information The online version contains supplementary material available at https://doi.org/10.1038/s42003-024-06693-6.

Correspondence and requests for materials should be addressed to Peng-Hua Fang or Wen-Bin Shang.

Peer review information *Communications Biology* thanks the anonymous reviewers for their contribution to the peer review of this work. Primary Handling Editors: Gabriela Da Silva Xavier and David Favero. A peer review file is available.